frontiers | Frontiers in Environmental Science

ORIGINAL RESEARCH
published: 12 August 2022
doi: 10.3389/fenvs.2022.921841

Study on Waste Acid Modificated Industrial Solid Waste Aluminum Ash to Prepare Environmental Functional Materials to Remove Fluoride Ions in Wastewater

Yuanchuan Ren[1,2], *Xiuping Chen*[1,2], *Guangfei Qu*[1,2]*, *Fenghui Wu*[1,2], *Yuyi Yang*[1,2], *Zuoliang Wang*[1,2], *Xinxin Liu*[1,2], *Caiyue Jin*[1,2] *and Yan Hu*[1,2]

[1]*Faculty of Environmental Science and Engineering, Kunming University of Science and Technology, Kunming, China,* [2]*National Regional Engineering Research Center-NCW, Kunming, China*

OPEN ACCESS

Edited by:
Vassilis Inglezakis, University of Strathclyde, United Kingdom

Reviewed by:
Maria Harja, Gheorghe Asachi Technical University of Iaşi, Romania
Su Xiaojuan, Southwest Forestry University, China
Antonis A. Zorpas, Open University of Cyprus, Cyprus

***Correspondence:**
Guangfei Qu
qgflab@sina.com

Specialty section:
This article was submitted to Water and Wastewater Management, a section of the journal Frontiers in Environmental Science

Received: *21 April 2022*
Accepted: *13 June 2022*
Published: *12 August 2022*

Citation:
Ren Y, Chen X, Qu G, Wu F, Yang Y, Wang Z, Liu X, Jin C and Hu Y (2022) Study on Waste Acid Modificated Industrial Solid Waste Aluminum Ash to Prepare Environmental Functional Materials to Remove Fluoride Ions in Wastewater. Front. Environ. Sci. 10:921841. doi: 10.3389/fenvs.2022.921841

C-SAAoa particles synthesized by simple and low-cost calcining industrial solid waste aluminium ash combined with waste oxalic acid modification process show excellent performance in fluoride removal speed and adsorption capacity. Their adsorption capacity on fluoride was determined at about 180.57 mg/g at pH 3.0, which was among the highest reported values in the literature. It was determined that the adsorption mechanism of fluoride on C-SAAoa particles followed mechanisms such as ion exchange, electrostatic action, and the surface - OH groups played a major role in the fluoride removal process. C-SAAoa particles can effectively remove fluoride, even in the presence of a certain concentration of competing anions. At the same time, the material possesses good cycling performance, and can still maintain 78.9% of the initial adsorption capacity in the longitudinal for eight recycles. Therefore, it may have the potential to become a promising adsorbent as a supplement to industrial solid waste resource-based utilization processes and also for fluoride removal in small-scale treatment facilities or wastewater with high fluoride concentrations.

Keywords: fluoride removal, industrial solid waste, waste oxalic acid, adsorption, resource utilization

1 INTRODUCTION

With the rapid development of the global chemical industry, the three industrial wastes (Lopez et al., 2022) and the sustainable development of resources (Constenla-Villoslada et al., 2022) have become one of the issues that are highly valued by all sectors of society, and at the same time have led to an increase in environmental problems (Wood and Wilcox, 2022). In the context of global industrialization, the large-scale production of solid waste (Huber et al., 2022) continuous consumption of resources have a significant impact on the natural environment and hinder sustainable development (Cortés et al., 2022). Because aluminum is second only to iron in terms of global metal demand, aluminum production is one of the major sources of solid waste (Wu et al., 2022). Aluminum ash is a hazardous solid waste formed by the reaction between molten aluminum and air during aluminum smelting and is divided into primary aluminum ash (Kashef-Haghighi et al., 2015) and secondary aluminum ash (SAA) (Aly et al., 2021). Primary aluminum ash contains nearly 80% aluminum and is usually recovered by remelting. The slag produced in this process is

called SAA. According to statistics, each ton of aluminum in the electrolysis, melting, casting and waste recycling process produces about 30–250 kg of SAA, while the utilization rate of SAA in China is only 40–50% (Zhu et al., 2022), and the production of SAA is also much greater than the consumption rate. About 95% of SAA ends up in landfills or is discarded near factories (Lee et al., 2022), posing a serious threat to the environment and human health.

In recent years, it has been recognized that the stabilization and recycling of waste is necessary to obtain the sustainability of the manufacturing process (Peters et al., 2019). The research of converting solid waste into adsorbent is one of the work of recycling resources. But today, research on the comprehensive utilization of SAA has mainly focused on inorganic materials such as construction and refractory materials (Bespolitov et al., 2021). For example, the formulation of non fired brick made of secondary aluminum ash was studied (Ni et al., 2022). Therefore, Further research in this field is warranted and the wider application of SAA needs to be further developed for better disposal and utilization of solid waste resources (Zhou et al., 2011).

Waste oxalic acid is produced by the bleaching process during pulping, paper making (Subbotina et al., 2021), textile and dyeing industries (Mu et al., 2022). The composition of waste oxalic acid (Levins and Smart, 1984)is very different from that of ordinary domestic wastewater (Li et al., 2022a) such as groundwater (Xie et al., 2022a) and municipal sewage (Larsson and Flach, 2021). It showed characteristic very low pH, high arsenic ion content, and other harmful ions. The existing waste acid treatment in industry (Hassan et al., 2021) mainly uses arsenic removal and neutralization processes, and there is still a indicated considerable room for improvement in terms of arsenic removal efficiency, stability of solid waste generated after arsenic removal (Silva and Mello-Castanho, 2007), and disposal cost (Lee et al., 2004).

Fluoride is an important element in flora and fauna (Ko et al., 2022). However, too much fluoride may inhibit plant metabolism, respiration and photosynthesis (Zhou et al., 2022). Excessive fluoride can also lead to dental fluorosis (Morris et al., 2022) and cause harm to the human body. Therefore, according to the World Health Organization (WHO, 2011) emission standards, the concentration of fluoride in drinking water should be targeted less than 1.5 mg/L (Gulegoda et al,. 2022), while the Chinese drinking water standard is 1.0 mg/L (Huang et al., 2022). More than 60 million people in more than 20 provinces in China have excess fluoride in their drinking water (Xiao et al,. 2022). In order to achieve major discharge targets for pollutants, many technologies have been reported for the removal of fluoride ions from wastewater (Alhassan et al., 2022), including chemical precipitation, ion exchange, reverse osmosis, nanofiltration, electro flocculation, and electro adsorption. Among them, adsorption technology (Ji et al., 2022) is the most commonly used technique due to its ease of operation, low price and adaptability. Adsorption materials are the key part of adsorption techniques (Xie et al., 2022b).

Although researchers have made great efforts in finding better fluoride adsorbents (Raghav et al., 2021), it is still challenging to develop effective and low-cost fluoride adsorbents. Considering the resource utilization of solid waste (Ge et al., 2022), the use of solid waste as a raw material for defluoridation and resource utilization of solid waste and the development of new environmentally functional materials based on solid waste (Kong et al., 2022) is an imperative strategy. Since solid waste is used as a raw material, the resulting adsorbent material can reduce the generation of solid waste and can contribute to sustainable development (Ullah and, Arslan, 2022). In this sense, this study proposes the concept of cheap, high-performance solid waste-based adsorbent materials to define adsorbent materials that consider resource recycling in the synthesis process. Recently, in order to solve the above problems, some researchers have been searching for new sources of materials. For adsorbent material sources, available solid wastes include SAA (Abbas et al., 2004), carbide slag (Yuan et al., 2018), carbon black (Wang and Cann, 2002), which can provide Ca^{2+}, Al^{3+}, and other metal ions to produce adsorbent materials. Synthesis of zeolites A and X from two industrial wastes: Crushed stone powder and aluminum ash (Kuroki et al., 2019). Preparation of nanofiber porous materials coated with aluminum ash by cellulose for effective adsorption of fluoride (Mahfoudhi and Boufi, 2020). Researcher (Yang et al., 2019) synthesis of Na-X zeolite from low aluminum coal fly ash: Characterization and high efficient As (V) removal. Meanwhile, the modification of SAA by using waste acids reduces the cost of waste acid treatment on the one hand, and slows down the pressure of SAA stockpiles on the other hand. Overall, many studies in this field have shown the feasibility of using cheaper and more readily available industrial solid waste aluminum ash as a favorable precursor for the production of advanced porous adsorbent materials in a highly feasible, economic and environmentally friendly manner (Long et al., 2022). This strategy allows the rational use of solid waste, thus reducing the environmental pollution (Yang et al., 2022a). However, studies on this direction are still scarce so far. Therefore, further study in this field is demanded.

In this paper, the precursor of fluoride adsorbent was prepared by calcination treatment of industrial solid waste aluminum ash, and waste acid was selected as the modifier. Different acid/aluminum molar ratios were investigated to determine the optimal ratio for fluoride removal. At the same time, different concentrations of waste acids are also used to improve the adsorption capacity. The properties of the related materials were investigated using SEM, EDS, XRD and FTIR. A number of adsorption experiments such as pH, adsorption isotherms, and adsorption kinetics have been carried out. The mechanism of adsorption was also elucidated. It provides a feasible route for the high value-added resource treatment of industrial solid waste aluminum ash and waste oxalic acid, and at the same time solves the problem of the source of high-performance fluoride removal adsorbent materials and reduces their treatment costs.

2 MATERIALS AND METHODS

2.1. Materials

Sodium fluoride, sodium chloride, sodium bromide, sodium nitrate, sodium sulfate, sodium phosphate, hydrochloric acid,

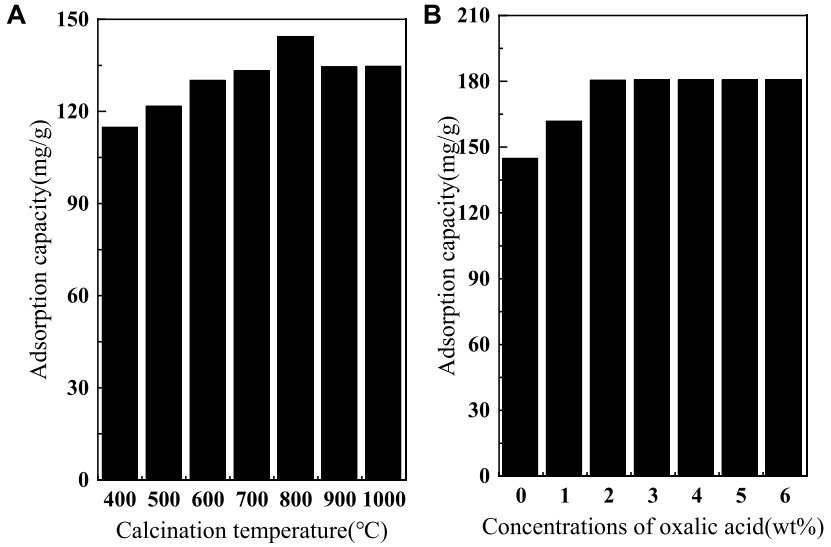

FIGURE 1 | (A) The calcination temperature of modified SAA, **(B)** fluoride removal effects of modified SAA with different concentrations of oxalic acid.

TABLE 1 | Specific surface area of SAA、C-SAA and C-SAA$_{oa}$.

Sorbent	BET surface area	Pore diameter (nm)	Pore volume
SAA	191.09 m^2/g	14.05	0.11 cm^3/g
C-SAA	276.12 m^2/g	16.07	0.15 cm^3/g
C-SAA$_{oa}$	335.38 m^2/g	18.36	0.17 cm^3/g

and sodium hydroxide were purchased from China Tianjin Zhiyuan Fine Chemical Co., Ltd (analytical grade). The aluminum ash (SAA) is taken from the electrolytic aluminum plant in Qujing Fuyuan, China, and the waste acid is taken from Beihai Printing & Dyeing Co., Ltd. in Shaoxing, Zhejiang, China (the main component is oxalic acid). Adjustment of solution pH with hydrochloric acid and sodium hydroxide as well as ultrapure water (conductivity: 18 MΩ) used throughout the process.

2.2. Preparation of C-SAA

The industrial solid waste SAA was placed in a muffle furnace at 400, 500, 600, 700, 800, 900°C and 1,000°Cfor 2 h and then decreased stepwise to room temperature. The cooled SAA was processed by ball-milled and sieving (200 mesh). Take $C_{(X°C)}$-SAA to remove fluoride, X = temperature of calcination.

2.3. Waste Oxalic Acid Modified C-SAA

Oxalic acid (concentrations of 0, 1, 2, 3, 3, 4, 5, 6%) was soaked for 12 h under sonication, then placed in a vacuum drying box at 60°C for 6 h to complete the modification of waste oxalic acid to C-SAA (C-SAAoa (Y%)).

2.4. Related Characterization

The compositions of the crystal structure were clarified using XRD (Rigaku ultimate 4, RIGAKU Co., Japan). The surface morphology of materials was determined by SEM (JSM-5800, Japan JEOL). The specific surface area of the materials were measured by BET (ASAP 2020,Micromeritics Co., United States) calculations. In addition, FTIR (IRTracer-100, SHIMADZU Co., Japan) spectra analysis was used to investigate the surface functional groups, recording in the range of 500–4,000 cm^{-1}.

2.5. Adsorption Experiments

Sodium fluoride were dissolved in ultrapure water to prepare a stock solution containing F (1,000 mg/L). Then, the concentration of the fluoride solution for the experiment is 100 mg/L. The conditions for these primary adsorption experiments were performed using 50 mg of adsorbent at pH 3.0 for 2 h OrionCHN090 fluoride ion selective electrode (Ortiz-Gomez et al., 1021) ere used to detect the concentration of fluoride. The fluoride removal efficiency (Riddell et al., 2022)was calculated using the following equation：

$$Qt = V(C_o - C_t)/m \quad (1)$$

where C_o (mg/L) and C_t (mg/L) are the initial and periodical fluoride ion concentrations in the fluoride ion solution, respectively. V (L) is 0.1 L and m (g) is the mass of the adsorbent.

Waste acid and sodium hydroxide in pH = 1–13 are used as modifiers, different pH values were determined. To better understand the adsorption process, adsorption isotherms from 10 to 1,000 ppm were studied at different temperatures (30, 40, 50°C). The obtained data were fitted to the Langmuir model (Zhang et al., 2022a) and the Freundlich model (Qu et al., 2022a). These models were shown as follows：

$$\text{Langmuir model: } \frac{C_e}{Q_e} = \frac{1}{Q_{max} \bullet b} + \frac{C_e}{Q_{max}} \quad (2)$$

$$\text{Freundlich model : } \ln(Q_e) = \ln\left(K_f\right) + \frac{1}{n}\ln(C_e) \quad (3)$$

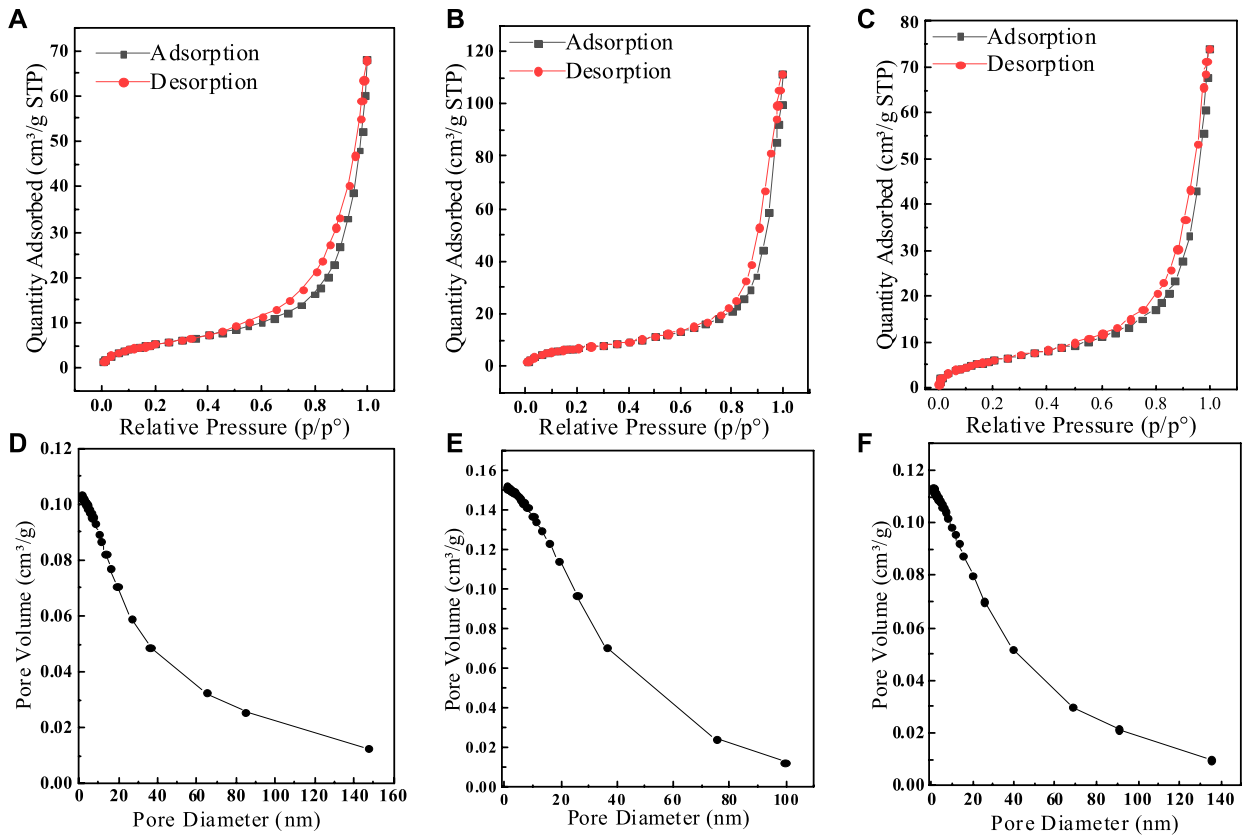

FIGURE 2 | (A) SAA,**(B)**C-SAA, **(C)** SAA_{oa} Nitrogen adsorption-desorption curve and **(D)** SAA, **(E)** C-SAA, **(F)** SAA_{oa} pore size distribution curve.

In **Eq. 2** and **Eq. 3**: Q_e (mg/g) is the equilibrium adsorption capacity, Q_{max} (mg/g) is the maximum adsorption capacity; C_e (mg/L) is the equilibrium arsenic concentration; b is the Langmuir adsorption constant; K_f is the Freundlich empirical constant; n is related to the heterogeneity of the adsorption energy site and intensity. The adsorption kinetics were studied for different temperatures (30, 40, 50°C) with reaction times ranging from5 to 240 min. Pseudo-first and pseudo-second order models were applied for the adsorption kinetic studies (Li et al., 2022b). Substituting these model equations into Eqs.

$$\text{Pseudo} - \text{first} - \text{order equation} : \ln(Q - Q_e) = \text{In}Q - K_1 t \quad (4)$$

$$\text{Pseudo} - \text{second} - \text{order equation} : t/Q_e = 1/K_2Q^2 + t/Q^2 \quad (5)$$

$$h = K_2Q^2 \quad (6)$$

In **Eq 4** and **Eq. 5** and **Eq. 6**:

C_o and C_t (mg/L) represent the initial concentration and concentration of fluoride ions at time t, respectively. V (L) is the volume of the solution, m (g) is the weight of the adsorbent; Q_e (mg/g) is the theoretical adsorption capacity at equilibrium, K_1 (1/min) and K_2 (g/(mg·min) are the pseudo-first-order and pseudo-second-order removal rate constants, respectively; Q_e (mg/g) is the adsorption capacity at equilibrium, C_e (mg/L) is the equilibrium concentration of fluoride ions, and Q (mg/g) is the maximum adsorption capacity of the adsorbent.

Different concentrations of anions were added to the fluoride solution (10, 30, 50, 100, 300, 500, mg/L). The anions included PO_4^{3-}, SO_4^{2-}, CO_3^{2-}, NO_3^-, CH_3COO^-, and Cl^-, showing the role of coexisting anions. Different concentrations of acid were used to estimate the recovery of the adsorbent material (Zeng et al,. 2022a) (0.1–8%). The regeneration performance of the material was studied for eight cycles (Yang et al., 2022b). Both $C_{(X°C)}$-SAA and C-SAAoa were applied to a batch of adsorption experiments to determine the performance of this modification.

3 RESULTS AND DISCUSSION

3.1. Effect of Calcination Temperature and Oxalic Acid

To demonstrate the effect of different calcination temperatures on the adsorption of fluoride by SAA, the effective of adsorption at different temperatures are presented in **Figure 1A**. The results showed that the adsorption amount increased rapidly with the increase of calcination temperature. The moderate increase in temperature significantly improved the removal of fluorine by SAA (Aumeier et al., 2022). When the calcination temperature is too high, the adsorption capacity decreases. The high temperature causes the original structure of SAA to be destroyed, and the substances in SAA melt and accumulate on the surface of the

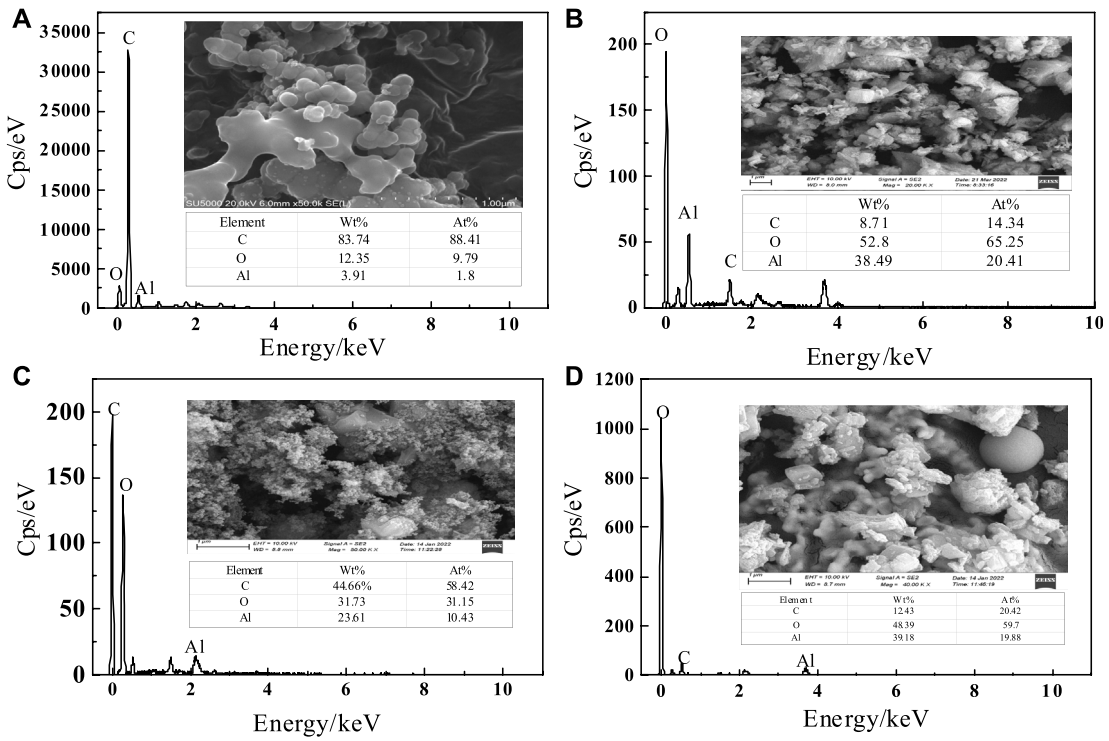

FIGURE3 | (A) SEM images and EDS spectra of C-SAA before adsorption, **(B)** SEM images and EDS spectra of C-SAA$_{oa}$ before adsorption, **(C)** SEM images and EDS spectra of C-SAA after adsorption, **(D)** SEM images and EDS spectra of C-SAA$_{oa}$ after adsorption.

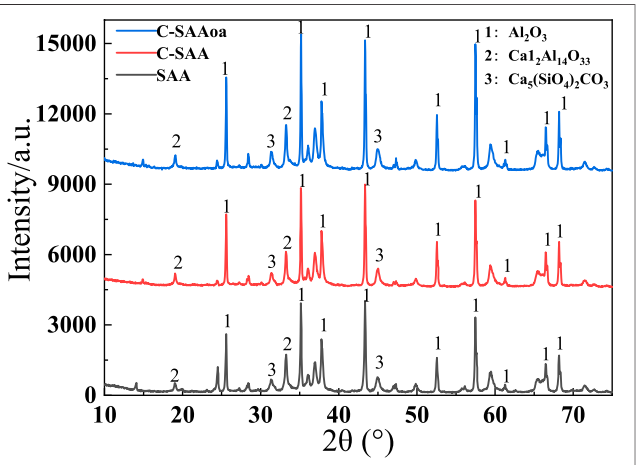

FIGURE 4 | The XRD spectra of SAA、C-SAA andC- SAA$_{oa}$.

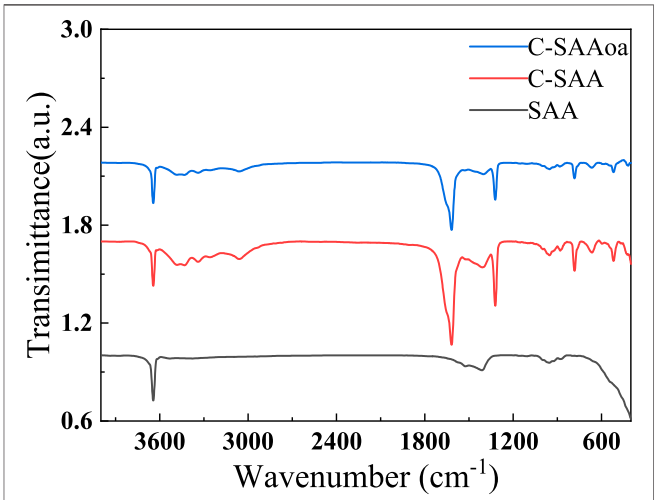

FIGURE 5 | The FTIR spectra of SAA、C-SAA and C-SAA$_{oa}$.

material or block the pores (Xu et al., 2022), resulting in a decrease in the specific surface area of the material (Yang et al., 2022c) and thus a decrease in the adsorption capacity. These results are displayed in **Table 1**. Due to the doping of oxalic acid, the O-atom content was increased after the modification. BET trial showed (shown in **Figure 2**) that calcination increased the specific surface area (276.12 m^2/g) relative to SAA (191.09 m^2/g), while $C_{(X°C)}$-SAA had a larger specific surface area, which was favorable for F^- to have sufficient adsorption site (Zhang et al., 2022b). Meanwhile, the specific surface of C-SAAoa was increased to 335.38 m^2/g. The pore size ranges from 0 to 40 nm and has mesoporous (Lv et al., 2022)properties, possessing certain adsorption advantages. Due to the addition of oxalic acid, the pore size and pore volume slightly increased (Bani-Atta, 2022). Interestingly, the best adsorption capacity of

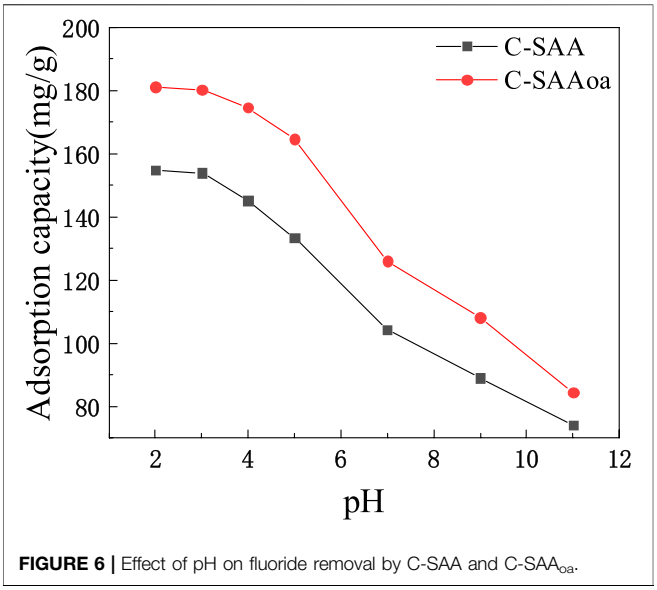

FIGURE 6 | Effect of pH on fluoride removal by C-SAA and C-SAA$_{oa}$.

$C_{(X°C)}$-SAA reached (144.38 mg/g) when the temperature of calcination was 800°C. Therefore, $C_{(800°C)}$-SAA, referred to as C-SAA in this paper, is used in the following experiments.

In addition, the adsorption capacity of modified C-SAA based on the surface strengthening effect of oxalic acid is shown in **Figure 1B**. It can be clearly seen that the oxalic acid-modified C-SAA showed different degrees of improvement in the adsorption capacity of fluorine compared to the unmodified material. The main reason is that the introduction of oxalic acid increases the amount of M-OH on the surface of C-SAA, increasing the probability of fluorine ion exchange with-OH through ion exchange (Karmakar et al., 2016). The removal capacity of fluorine increased with the increase of oxalic acid concentration. The maximum fluoride removal capacity was reached at 2% oxalic acid concentration. When the oxalic acid concentration continued to increase and was greater than 2%, the fluoride removal capacity remained basically the same. The results showed that C-SAA was completely modified when the mass fraction of oxalic acid was 2%, and the adsorption capacity was about 180.42 mg/g. Considering the amount of oxalic acid and its modification effect, an oxalic acid solution with a mass fraction of 2% can be considered as a chemical impregnation modifier (Zhao et al., 2022) for modified C-SAA, which is referred to as C-SAAoa in this paper (as the nomenclature in 2.2 and 2.3).

3.2. Characterization of SAA、C-SAA and C-SAAoa

To understand the changes of oxalic acid action, SEM-EDS plots of C-SAA and C-SAAoa before and after fluoride adsorption are shown in **Figures 3A–D**. The surface of the material was rough and presented as a multidimensional lamellar stacking structure (Li et al., 2021a) (**Figure 2A**), and the modified material showed a dispersed distribution (**Figure 2B**). After adsorption, the material has a spherical cluster structure (Zhang et al., 2022c). EDS analysis demonstrated that the main constituent elements of

TABLE 2 | Isotherm parameters for the Freundlich model at different temperatures about C-SAA and C-SAA$_{oa}$.

Temperature (°C)	K_F	n	R^2
C-SAA			
30	4.244	1.716	0.9493
40	5.527	1.679	0.9594
50	7.334	1.648	0.9637
C-SAA$_{oa}$			
30	13.497	2.251	0.9869
40	15.595	2.083	0.9880
50	18.096	1.979	0.9892

C-SAA are C, O and Al. The XRD results of C-SAA and C-SAAoa are shown in **Figure 4**. Diffraction peaks corresponding to Al_2O_3 are found at 2θ = 25.58°, 35.129°, 37.782°and 43.369° (Fujita et al., 2022) (JCPDScard74-1895), indicating the presence of Al_2O_3 in the material. C-SAA retained its original crystal structure after oxalic acid impregnation. And at 14.89° and 47.36°, two faint new diffraction peaks appeared, which may be oxalic acid hydroxyl groups generated on the surface of the modified material (Lubkowicz et al., 2022).

The infrared spectra of these materials are shown in **Figure 5**. C-SAA has characteristic peaks at 3,313, 3,092, 1,644, 1,157, 1,075, 737, 609 and 479 cm^{-1} before adsorption, which corresponds to the absorption peaks at 3,296, 3,094, 1,640, 1,164, 1,071, 751, 630 and 484 cm^{-1} for γ-AlOOH (Bai et al., 2021) mentioned in the literature. The modified C-SAAoa material showed absorption peaks at 3,309, 3,095, 1,623, 1,167, 1,080, 743, 606 and 483 cm^{-1}. After modification by oxalic acid impregnation, the material was displaced at the position of the original absorption peak (Karmakar et al., 2016) of C-SAAoa, confirming the formation of the modified C-SAAoa. Due to calcination at 800°C, the material was displaced at the position of the original absorption peak of C-SAA, confirming the formation of C-SAA. The absorption peak at 1,075 cm^{-1} belongs to the characteristic peak of Al-OH (Zhang et al., 2022d), indicating that calcination led to the hydroxylation of the material surface (Wang et al., 2022a) and that C-SAA is rich in hydroxyl sites. C-SAAoa also has a sharp absorption peak at 1,071 cm^{-1}, which belongs to the characteristic peak of Al-OH, indicating that the modified C-SAAoa is rich in hydroxyl sites (Li et al., 2021b). C-SAAoa showed a sharp new absorption peak at 1,315 cm^{-1} belonging to C=O (Qu et al., 2022b), indicating the possible presence of hydroxy oxalate on the surface of C-SAAoa.

3.3. Effect of pH

The effect of initial solution pH on C-SAA and C-SAAoa on F^-adsorption is shown in **Figure 6**. In fluoride ion removal studies using C-SAA and C-SAAoa, pH exerted a large influence on the process. When the pH was two to three, the adsorption amount of C-SAA was about 154 mg/g and the adsorption amount of C-SAAoa was about 180 mg/g. When the pH was increased from 3 to 7, the adsorption of C-SAA decreased from 154 mg/g to 104.28 mg/g and the adsorption of C-SAAoa decreased from 180 mg/g to 125.93 mg/g. The

adsorption capacity of these materials decreases sharply at pH = 7–11. These materials have good fluoride removal properties over a wide pH range (Hosseini et al., 2020), and the acidic pH favors fluoride adsorption. Then other adsorption experiments were performed at pH = 3. Compared with C-SAA, the adsorption capacity of modified C-SAAoa in pH = two to seven was increased by 14–23%. The effect of pH on fluoride removal mainly includes the effects of competitive adsorption (Zhu et al., 2010)and electrostatic attraction (Hamilton et al., 2022). The higher adsorption of the material at acidic pH is mainly due to the competitive adsorption of OH^- and less electrostatic adsorption of H^+ (Zhang et al., 2022e). Thus, it promotes the exchange of ionophores between F^- and Me-OH (Wang et al., 2022b). With the increase of pH, the competitive adsorption of F^- and OH^- resulted in a decreasing trend of adsorption. That is, the higher the concentration of OH^-, the more obvious the competitive adsorption effect. The addition of oxalic acid can significantly increase the electrostatic attraction and will successfully weaken the competitive adsorption (Karmakar et al., 2016), which corresponds to the zeta potential of C-SAA and C-SAAoa.

3.4. Adsorption Thermodynamics

To further investigate the effect of initial fluoride ion concentration on fluoride ion removal, we performed adsorption thermodynamic experiments on C-SAA and C-SAAoa. We fitted the experimental data using the Langmuir and Freundlich models, respectively. It is obvious from **Figure 7** that the Freundlich model is more suitable than the Langmuir model for this experimental data. The relevant thermodynamic parameters of the Freundlich model are shown in **Table 2**. The high values of regression coefficients for C-SAA and C-SAAoa (R^2 = 0.9493–0.9892) indicate that the experimental results are consistent with the Freundlich adsorption isotherm. This may be due to the fact that different adsorption sites on the material surface have different adsorption energies (Chen et al,. 2022a), further illustrates a correlation with oxalic acid modification of C-SAA. The major hydroxyl sites (Zhang et al., 2022e) on the surface of C-SAA and C-SAAoa, such as Al-OH and M-OH, have different adsorption energies. In addition, the n values obtained from the fitted curves were all greater than 1, indicating a strong affinity (Li et al., 2021b) (F^-) between the adsorbent and the adsorbate. This indicates that the adsorption process is not simple physical adsorption, but chemisorption with the formation of stable chemical bonds (MF) (Liao et al., 2022). The n-value of C-SAAoa is greater than the n-value of C-SAA, indicating that the fluoride concentration had a greater effect on C-SAAoa. As the temperature of the experiment

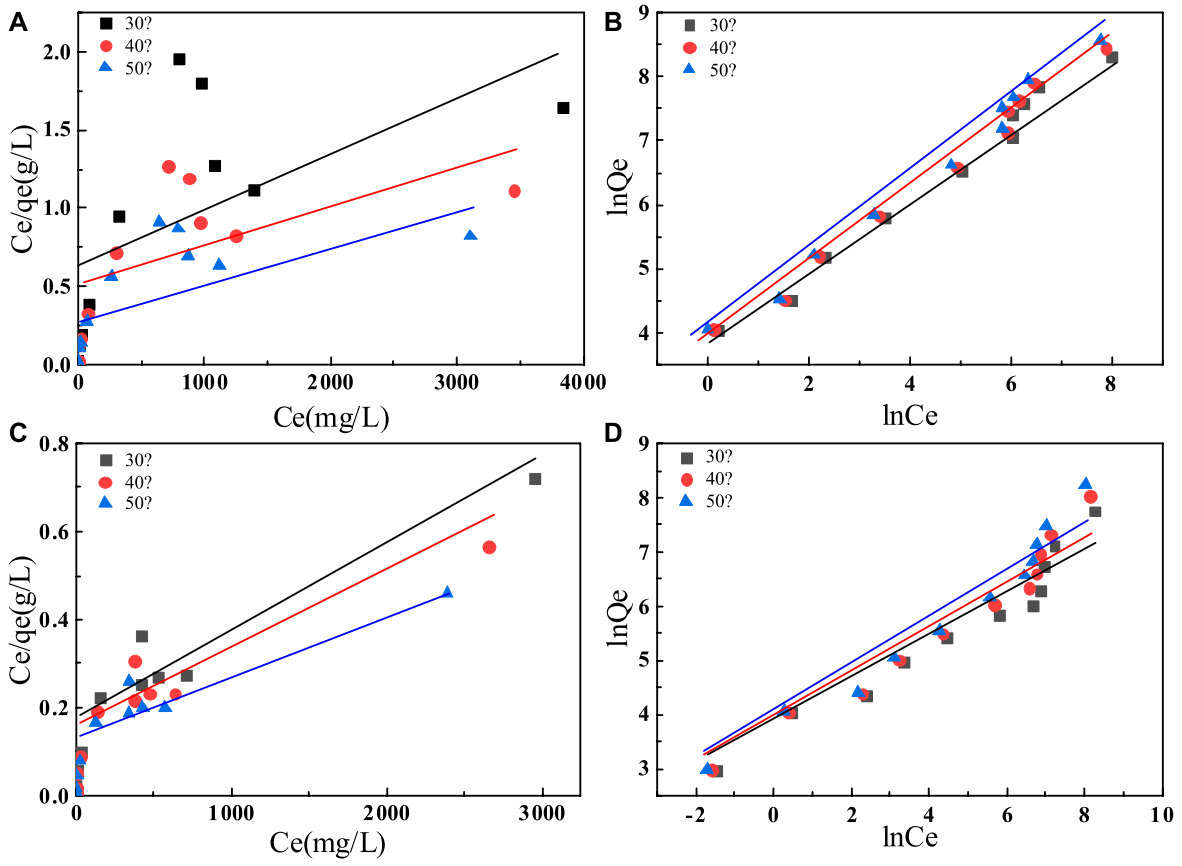

FIGURE 7 | Adsorption isotherm models of fluoride on C-SAA **(A)** the Langmuir model; **(B)** the Freundlich model; adsorption isotherm model of fluoride on C-SAAoa**(C)** the Langmuir model; **(D)** the Freundlich model.

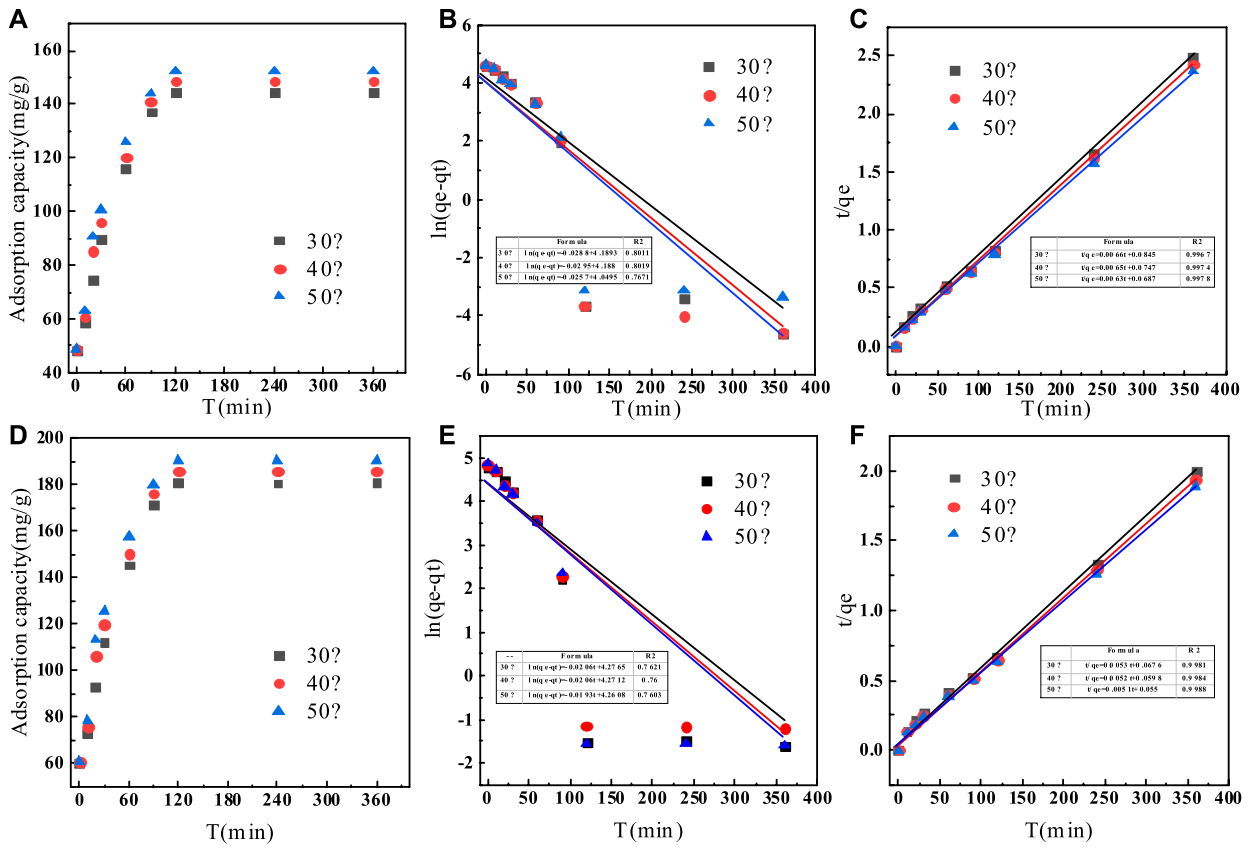

FIGURE 8 | (A) Adsorption kinetics of fluoride on C-SAA; **(B)** the pseudo-fifirst-order model on C-SAA; **(C)** the pseudo-second-order model on C-SAA; **(D)** adsorption kinetics of fluoride on C-SAA$_{oa}$; **(E)** the pseudo-fifirst-order model on C-SAA$_{oa}$; **(F)** the pseudo-second-order model on C-SAA$_{oa}$.

increases, the K_F values also increased, indicating that temperature has a facilitative effect on the adsorption process, further demonstrating that the adsorption process is a heat-absorbing reaction (Cao et al., 2022). The higher the value of K_F, the stronger the combined ability reflected. Therefore, the binding of fluorine to C-SAAoa is easier than that of C-SAA.

3.5. Adsorption Kinetics

The adsorption kinetics were studied by the effect of adsorption reaction time on the defluorination of C-SAA and C-SAAoa. The results are shown in **Figure 8**. The faster adsorption rate (Querejeta et al., 2022) of fluoride ions in the material can be found by **Figures 8A,D**. During the first 30 min, the adsorption process was very rapid (Zeng et al., 2022b). The adsorption capacity of C-SAA increased dramatically, reaching 89.70, 95.78 and 100.50 mg/g, respectively. The adsorption capacities of C-SAAoa reached 112.12, 119.73 and 125.62 mg/g in 30 min, respectively. Although the adsorption rate slowed down in 30 min~1h, it still maintained a high adsorption rate. The adsorption rate leveled off in 1–2 h and reached adsorption equilibrium in about 2 h. The equilibrium adsorption amounts of C-SAA were 144.46, 148.43 and 152.34 mg/g, respectively. The equilibrium adsorption amounts of C-SAAoa were 180.57, 185.54 and 190.43 mg/g, respectively. As apparent from **Figure 8**, with the increase of temperature, the adsorption rate accelerates and the equilibrium adsorption amount increases (Davarpanah et al., 2022). Therefore, it can be concluded that the process of C-SAA and C-SAAoa defluorination is a heat absorption process (Hou et al., 2022). Compared with the equilibrium adsorption capacity of C-SAA, the fluoride removal capacity of C-SAAoa was increased by 15–25%. Pseudo-first-order kinetics model and pseudo-second-order kinetics model were used to fit the data. The fitting results are shown in **Figures 8B,C,E,F**. The data match the pseudo-second-

TABLE 3 | Kinetic parameters for the pseudo-second-order models at different temperatures about C-SAA and C-SAAoa.

Temperature (°C)	Qe (mg/g)	$K_2 \times 10^3$ (g/mg·min)	R^2
C-SAA			
30	144.46	4.48	0.9981
40	148.43	4.77	0.9984
50	152.34	6.78	0.9988
C-SAA$_{oa}$			
30	180.57	1.76	0.9967
40	185.54	1.98	0.9974
50	190.43	2.50	0.9978

TABLE 4 | Comparison of the adsorption capacity of fluoride by C-SAAoa with other adsorbents.

Adsorbent	pH	Adsorption (mg/g)	Ref
Zeolite/hydrous aluminum oxide synthesized from coal fly ash	6.0	18.12	Chen et al. (2022b)
Aluminum hydroxide modified porous cellulose aerogel	5.0	35	Mahfoudhi and Boufi, (2020)
Al_2O_3/Carbon nanotubes	5.0–7.0	28.7	Li et al. (2001)
Basic aluminium sulfate@graphene	7.0	33.4	Chen et al. (2013)
Alum-impregnated activated alumina	6.5	40.3	Tripathy et al. (2006)
Tantalum Hydroxide	2	78.5	Yu et al. (2012)
am-ZrO_2	6.2	99.01	Su et al. (2013)
FeeZr binary oxide	5.5	102.3	Ren et al. (2012)
C-SAA_{oa}	3.0	180.57	Present study

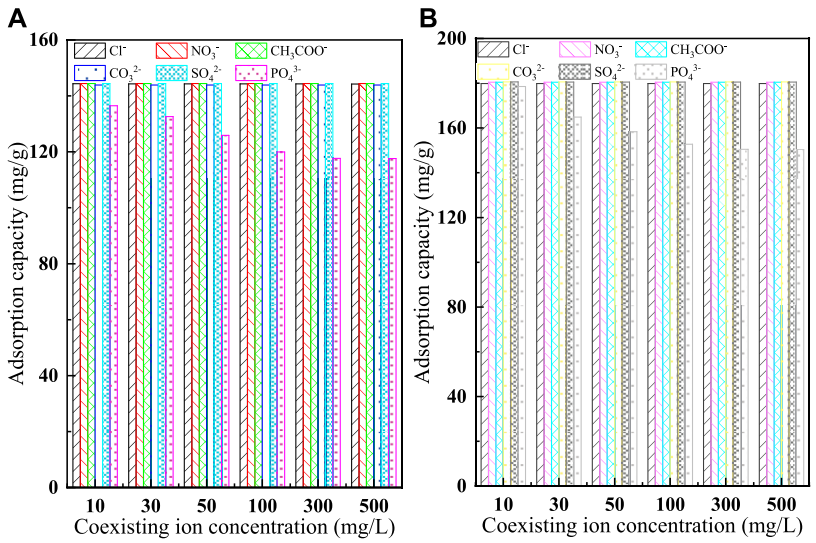

FIGURE 9 | Effect of coexisting anions on the adsorption of fluoride about C-SAA and C-SAAoa.

order kinetic model and their associated dynamic models well. The parameters of the pseudo-secondary model are shown in **Table 3**. Due to the high correlation coefficient (R^2 = 0.9967–0.9988), the kinetics of fluorine removal by C-SAA and C-SAAoa were well described using a pseudo-secondary model, indicating that the surface adsorption (Gupta et al., 2022)reaction is the dominant and control phase and the rate control step is chemisorption. The smaller the k_2 value, the more the number of adsorption sites (Du et al., 2022). Thus, the introduction of oxalic acid significantly improved the exchange capacity of -OH and F^- on the adsorbent surface. Comparison of the adsorption capacity of fluoride by C-SAAoa with other adsorbents are shown in **Table 4**.

3.6. Effect of Coexisting Anions

In natural water and wastewater containing fluoride, multiple anions are usually present (Krivina et al., 2022), such as Cl^-, NO_3^-, CH_3COO^-, CO_3^{2-}, SO_4^{2-}, and PO_4^{3-}. The presence of coexisting ions can lead to competition with adsorbent ions for adsorption sites during adsorption, reducing the removal efficiency of the target pollutant. The strength of the adsorption competition for coexisting anions depends mainly on the relative ionic concentration and its affinity to the adsorbent, while the magnitude of the affinity is closely related to the ionic radius and charge (Bakhta et al., 2022). In this experiment, the effects of different concentrations (10 mg/L, 30 mg/L, 50 mg/L, 100 mg/L, 300 mg/L, 500 mg/L) of Cl^-, NO_3^-, CH_3COO^-, CO_3^{2-}, SO_4^{2-} and PO_4^{3-} on the adsorption behavior of fluoride ions were investigated. The results are shown in **Figure 9**. From the plot it is easy see that except for PO_4^{3-}, the remaining five anions have little effect on the adsorption of fluoride ions by C-SAA and C-SAAoa. With the increase of PO_4^{3-} concentration, the removal of F^- by C-SAA decreased to 94.45%, 91.77%, 87.13%, 83.06%, 81.44 and 81.38%, respectively, while the removal of F^- by C-SAAoa decreased to 98.87%, 91.31%, 87.68%, 84.60%, 83.31 and 83.27%, respectively. This phenomenon is mainly due to the high density of negative charge of PO_4^{3-} (Cha et al., 2022), resulting in its easy adsorption on the surface of positively charged materials. PO_4^{3-} (3/3.40) and F^- (1/1.33) possess similar charge radii. PO_4^{3-} in solution can gradually occupy the active adsorption sites on the adsorbent surface (Wang et al., 2022c), making the adsorbent unable to accept

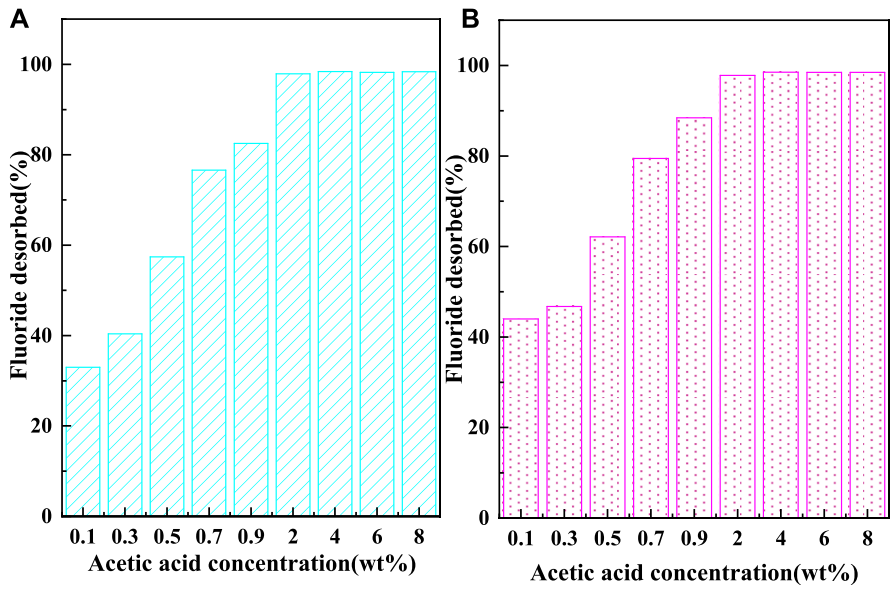

FIGURE 10 | Effect of oxalic acid concentration on the desorption of fluoride about C-SAA and C-SAAoa.

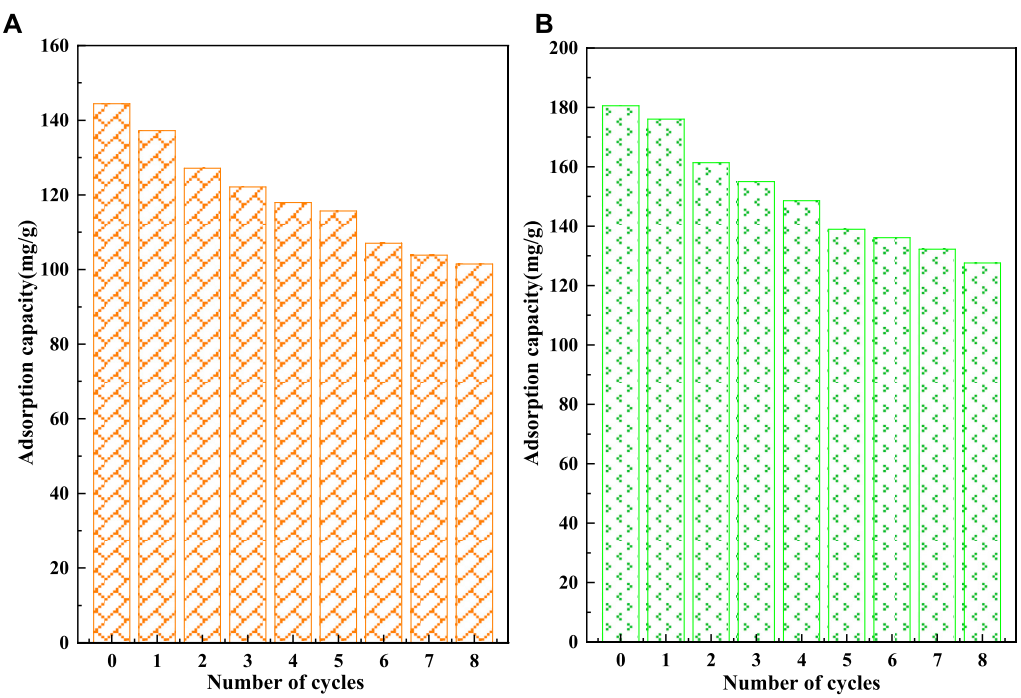

FIGURE 11 | Effect of cyclic adsorption-regeneration runs on the adsorption of fluoride about C-SAA and C-SAAoa.

more F^-. Therefore, when large amounts of PO_4^{3-} and F^- are present in the solution, we may wish to use the simultaneous removal treatment method. In contrast, C-SAA and C-SAAoa are more selective for F^- than PO_4^{3-} in water, and the adsorption process is not susceptible to other disturbances to coexisting anions.

3.7. Regeneration

The recycling performance of C-SAA and C-SAAoa is shown in **Figures 10**, **11**. The F^- adsorbed on the material can be desorbed by acids, bases, salts, etc (Wagstaff and Petrie, 2022). In order to ensure the adsorption performance of the adsorbent after desorption, the choice of the desorbent depends largely on the

-OH content. In this experiment, acetic acid solution with abundant carboxyl groups and weak acidity was chosen as the desorption agent (Li et al., 2021b). The desorption effect of F^- at different oxalic acid concentrations is shown in **Figure 10**. With the increase of acetic acid concentration, the desorption rates of F^- gradually increased and leveled off. When the oxalic acid concentration continues to increase to 2%, the desorption effect will not change, which is caused by the limited adsorption sites occupied by fluorine ions in the material. The results of the 8-cycle adsorption-desorption experiment are shown in **Figure 11**. The adsorption of C-SAA and C-SAAoa on F^- decreased gradually as the number of cycles increased, but still maintained good adsorption capacity at the eighth cycle. They both maintained 78.9 and 78.3% of the initial adsorption capacity. In conclusion, C-SAA and C-SAAoa have good recirculation performance for the adsorption of F^-.

3.8. Mechanism of Adsorption

The fluorine removal mechanism reaction formula of C-SAA and C-SAAoa is shown in (7–11). 1) Electrostatic action (Song et al., 2022):C-SAA and C-SAAoa adsorb fluoride ions to the surface of the material by electrostatic attraction. 2) Coordination (Hempelmann et al., 2022):Fluoride ions form Al-F complexes with Al on the surface of C-SAA and C-SAAoa. 3) Ion exchange (Jiang et al., 2022): The generation of M-F complexes releases hydroxyl radicals and forms stable AlO-F, CO-F bonds. Thus, the mechanism of fluoride adsorption and removal by C-SAA and C-SAAoa includes a combination of electrostatic interactions, coordination and ion exchange effects. The chemical reactions are shown below:

Electrostatic effect：

$$\mathrm{A1OOHH^+ + F^- \rightarrow A1OOHHF} \quad (7)$$

$$\mathrm{HOOCCOOH + F^- \rightarrow HOOCCOOHF} \quad (8)$$

Coordination：

$$\mathrm{A1OOH + F^- \rightarrow F - A1OOH} \quad (9)$$

Ion exchange:

$$\mathrm{A1OOH + F^- \rightarrow A1O - F + OH} \quad (10)$$

$$\mathrm{HOOCCOOH + F^- \rightarrow HOOCCOF + OH} \quad (11)$$

4. CONCLUSION

In summary, C-SAAoa particles synthesized by simple and low-cost calcining industrial solid waste aluminium ash combined with waste oxalic acid modification process show excellent performance in fluoride removal speed and adsorption capacity. Their adsorption capacity on fluoride was determined at about 180.57 mg/g at pH 3.0, which was among the highest reported values in the literature. It was determined that the adsorption mechanism of fluoride on C-SAAoa particles followed mechanisms such as ion exchange, electrostatic action, and the surface -OH groups played a major role in the fluoride removal process. C-SAAoa particles can effectively remove fluoride, even in the presence of a certain concentration of competing anions. At the same time, the material possesses good cycling performance, and can still maintain 78.9% of the initial adsorption capacity in the longitudinal for eight recycles. Therefore, it may have the potential to become a promising adsorbent as a supplement to industrial solid waste resource-based utilization processes and also for fluoride removal in small-scale treatment facilities or wastewater with high fluoride concentrations.

DATA AVAILABILITY STATEMENT

The original contributions presented in the study are included in the article/supplementary material, further inquiries can be directed to the corresponding author.

AUTHOR CONTRIBUTIONS

QG is responsible for writing the article, and RY is responsible for providing data and drawings.

FUNDING

Financial support for this project was provided by The National Key Research and Development Plan-Ecological Link Technology for Clean processing of Typical by-products of Unconventional Wet/thermal Production (2018YFC1900203).

ACKNOWLEDGMENTS

The National Key Research and Development Plan- The environmental functional materials of long-acting solidification/stabilizer for heavy metal tailings pollution, technologies and equipment etc (2018YFC1801702), which is greatly acknowledged.

REFERENCES

Abbas, A., Fadel, P. J., Wang, Z. Y., Arbique, D., Jialal, I., Vongpatanasin, W. P., et al. (2004). Contrasting effects of oral versus transdermal estrogen on serum amyloid A (SAA) and high-density lipoprotein-SAA in postmenopausal women. *Arterioscler. Thromb. Vasc. Biol.* 24, E164–E167. doi:10.1161/01.atv.0000140198.16664.8e

Alhassan, S. I., Wang, H. Y., He, Y. J., Yan, L. J., Jiang, Y. X., Wu, B. C., et al. (2022). Fluoride remediation from on-site wastewater using optimized bauxite nanocomposite (Bx-Ce-La@500): Synthesis maximization, and mechanism of F- removal. *J. Hazard. Mater.* 430, 128401. doi:10.1016/j.jhazmat.2022.128401

Aly, N. A., Casillas, G., Luo, Y.-S., McDonald, T. J., Wade, T. L., Zhu, R., et al. (2021). Environmental impacts of hurricane florence flooding in eastern North Carolina: Temporal analysis of contaminant distribution and potential human

health risks. *J. Expo. Sci. Environ. Epidemiol.* 31, 810–822. doi:10.1038/s41370-021-00325-5

Aumeier, B. M., Augustin, A., Thones, M., Sablotny, J., Wintgens, T., Wessling, M., et al. (2022). Linking the effect of temperature on adsorption from aqueous solution with solute dissociation. *J. Hazard. Mater.* 429, 128291. doi:10.1016/j.jhazmat.2022.128291

Bai, L. F., Xu, K. Z., Jiang, W. Q., Sang, M., Fang, Q. L., Xuan, S. H., et al. (2021). Spatially ensemble of polydopamine-protected-Au nanocrystals on Fe3O4@SiO2@γ-AlOOH microflower for improving catalytic performance. *Appl. Surf. Sci.* 543, 148750. doi:10.1016/j.apsusc.2020.148750

Bakhta, S., Sadaoui, Z., Bouazizi, N., Samir, B., Allalou, O., Devouge-Boyer, C., et al. (2022). Functional activated carbon: From synthesis to groundwater fluoride removal. *RSC Adv.* 12, 2332–2348. doi:10.1039/d1ra08209d

Bani-Atta, S. A. (2022). Potassium permanganate dye removal from synthetic wastewater using a novel, low-cost adsorbent, modified from the powder of Foeniculum vulgare seeds. *Sci. Rep.* 12, 4547. doi:10.1038/s41598-022-08543-z

Bespolitov, D. V., Konovalova, N. A., Dabizha, O. N., Pankov, P. P., and Rush, E. A. (2021). Influence of the mechanical activation of fly ash on strength of ground concrete based on waste production. *Ekol. Prom. Ross.* 25, 36–41. doi:10.18412/1816-0395-2021-11-36-41

Cao, T. Y., Lee, W., Huang, R. J., Gorte, R. J., and Vohs, J. M. (2022). Liquid-Organic hydrogen carriers as endothermic fuels. *Fuel* 313, 123063. doi:10.1016/j.fuel.2021.123063

Cha, S., Cho, Y., Kim, J. G., Choi, H., Ahn, D., Sun, J., et al. (2022). Controllable triboelectric series using gradient positive and negative charge-confinement layer with different particle sizes of mesoporous carbon materials. *Small methods* 6, e2101545. doi:10.1002/smtd.202101545

Chen, J. B., Yang, R. J., Zhang, Z. Y., and Wu, D. Y. (2022a). Removal of fluoride from water using aluminum hydroxide-loaded zeolite synthesized from coal fly ash. *J. Hazard. Mater.* 421, 126817. doi:10.1016/j.jhazmat.2021.126817

Chen, W. Y., Cao, J. B., Fu, W. Z., Zhang, J., Qian, G., Yang, J., et al. (2022b), *Molecular-level insights into the notorious CO poisoning of platinum catalyst*. German: Angewandte Chemie-International Edition.

Chen, Y., Zhang, Q., Chen, L., Bai, H., and Li, L. (2013). Basic aluminum sulfate@graphene hydrogel composites: Preparation and application for removal of fluoride. *J. Mat. Chem. A Mat.* 1, 13101. doi:10.1039/c3ta13285d

Constenla-Villoslada, S., Liu, Y., Wen, J., Sun, Y., and Chonabayashi, S. (2022). Large-scale land restoration improved drought resilience in Ethiopia's degraded watersheds. *Nat. Sustain.* 5, 488–497. doi:10.1038/s41893-022-00861-4

Cortés, E., Grzeschik, R., Maier, S. A., and Schlücker, S. (2022). Experimental characterization techniques for plasmon-assisted chemistry. *Nat. Rev. Chem.* 6, 259–274. doi:10.1038/s41570-022-00368-8

Davarpanah, M., Rahmani, K., Kamravaei, S., Hashisho, Z., Crompton, D., Anderson, J. E., et al. (2022). Modeling the effect of humidity and temperature on VOC removal efficiency in a multistage fluidized bed adsorber. *Chem. Eng. J.* 431, 133991. doi:10.1016/j.cej.2021.133991

Du, J. H., Chen, L., Zhang, B., Chen, K. Z., Wang, M., Wang, Y., et al. (2022). Identification of CO2 adsorption sites on MgO nanosheets by solid-state nuclear magnetic resonance spectroscopy. *Nat. Commun.* 13, 707. doi:10.1038/s41467-022-28405-6

Fujita, Y., Niizeki, T., Fukumitsu, N., Ariga, K., Yamauchi, Y., Malgras, V., et al. (2022). Mechanisms responsible for adsorption of molybdate ions on alumina for the production of medical radioisotopes. *Bull. Chem. Soc. Jpn.* 95, 129–137. doi:10.1246/bcsj.20210249

Ge, J. H., Xiao, Y. H., Kuang, J., and Liu, X. M. (2022). Research progress of chlorination roasting of heavy metals in solid waste. *Surfaces Interfaces* 29, 101744. doi:10.1016/j.surfin.2022.101744

Gulegoda, C. R., Dissanayake, C. B., Amarasekara, D. S., Wijeratne, S., Premadasa, J. K., Chandrajith, R., et al. (2022), *Impact of fluoride exposure on male reproductive parameters: A pilot case-control study in Sri Lanka*. Sri Lanka: Exposure and Health.

Gupta, S., Anh Nguyen, N., and Muhich, C. L. (2022). Surface water H-bonding network is key controller of selenate adsorption on 012 alpha-alumina: An *ab-initio* study. *J. colloid interface Sci.* 617, 136–146. doi:10.1016/j.jcis.2022.02.128

Hamilton, I., Gebala, M., Herschlag, D., and Russell, R. (2022). Direct measurement of interhelical DNA repulsion and attraction by quantitative cross-linking. *J. Am. Chem. Soc.* 144, 1718–1728. doi:10.1021/jacs.1c11122

Hassan, G., Shabbir, M. A., Ahmad, F., Pasha, I., Aslam, N., Ahmad, T., et al. (2021). Cereal processing waste, an environmental impact and value addition perspectives: A comprehensive treatise. *Food Chem.* 363, 130352. doi:10.1016/j.foodchem.2021.130352

Hempelmann, J., Muller, P. C., Ertural, C., and Dronskowski, R. (2022). The orbital origins of chemical bonding in Ge-Sb-Te phase-change materials. *Angew. Chem.-Int. Ed.* 61, e202115778. doi:10.1002/anie.202115778

Hosseini, M., Esrafili, A., Farzadkia, M., Kermani, M., and Gholami, M. (2020). Degradation of ciprofloxacin antibiotic using photo-electrocatalyst process of Ni-doped ZnO deposited by RF sputtering on FTO as an anode electrode from aquatic environments: Synthesis, kinetics, and ecotoxicity study. *Microchem. J.* 154, 104663. doi:10.1016/j.microc.2020.104663

Hou, Y. L., Sheng, Z. Z., Fu, C., Kong, J., and Zhang, X. T. (2022). Hygroscopic holey graphene aerogel fibers enable highly efficient moisture capture, heat allocation and microwave absorption. *Nat. Commun.* 13, 1227. doi:10.1038/s41467-022-28906-4

Huang, L. W., Sun, Z. Y., Zhou, A. G., Bi, J. B., and Liu, Y. D. (2022). Source and enrichment mechanism of fluoride in groundwater of the hotan oasis within the tarim basin, northwestern China. *Environ. Pollut.* 300, 118962. doi:10.1016/j.envpol.2022.118962

Huber, B., Larsen, T., Spengler, R. N., and Boivin, N. (2022). *How to use modern science to reconstruct ancient scents*. Berlin: Nature Human Behaviour.

Ji, Y., Chen, Z., Wei, R., Yang, C., Wang, Y., Xu, J., et al. (2022). Selective CO-to-acetate electroreduction via intermediate adsorption tuning on ordered Cu–Pd sites. *Nat. Catal.* 5, 251–258. doi:10.1038/s41929-022-00757-8

Jiang, S. X., Li, Q. R., Jia, W. T., Wang, F., Cao, X. Y., Shen, X. B., et al. (2022). Expanding the application of ion exchange resins for the preparation of antimicrobial membranes to control foodborne pathogens. *Chemosphere* 295, 133963. doi:10.1016/j.chemosphere.2022.133963

Karmakar, S., Dechnik, J., Janiak, C., and De, S. (2016). Aluminium fumarate metal-organic framework: A super adsorbent for fluoride from water. *J. Hazard. Mater.* 303, 10–20. doi:10.1016/j.jhazmat.2015.10.030

Kashef-Haghighi, S., Shao, Y. X., and Ghoshal, S. (2015). Mathematical modeling of CO2 uptake by concrete during accelerated carbonation curing. *Cem. Concr. Res.* 67, 1–10. doi:10.1016/j.cemconres.2014.07.020

Ko, A., Banks, J. T., Hill, C. M., and Chi, D. L. (2022). Fluoride prescribing behaviors for medicaid-enrolled children in Oregon. *Am. J. Prev. Med.* 62, E69–E76. doi:10.1016/j.amepre.2021.06.016

Kong, H., Chen, Y., Yang, G. Z., Liu, B., Guo, L., Wang, Y., et al. (2022). Two-dimensional material-based functional aerogels for treating hazards in the environment: Synthesis, functional tailoring, applications, and sustainability analysis. *Nanoscale Horiz.* 7, 112–140. doi:10.1039/d1nh00633a

Krivina, R. A., Lindquist, G. A., Yang, M. C., Cook, A. K., Hendon, C. H., Motz, A. R., et al. (2022). Three-electrode study of electrochemical ionomer degradation relevant to anion-exchange-membrane water electrolyzers. *ACS Appl. Mat. Interfaces* 14, 18261–18274. doi:10.1021/acsami.1c22472

Kuroki, S., Hashishin, T., Morikawa, T., Yamashita, K., and Matsuda, M. (2019). Selective synthesis of zeolites A and X from two industrial wastes: Crushed stone powder and aluminum ash. *J. Environ. Manag.* 231, 749–756. doi:10.1016/j.jenvman.2018.10.082

Larsson, D. G. J., and Flach, C.-F. (2021). Antibiotic resistance in the environment. *Nat. Rev. Microbiol.* 20, 257–269. doi:10.1038/s41579-021-00649-x

Lee, B. K., Ellenbecker, M. J., and Moure-Ersaso, R. (2004). Alternatives for treatment and disposal cost reduction of regulated medical wastes. *Waste Manag.* 24, 143–151. doi:10.1016/j.wasman.2003.10.008

Lee, K. H., Qasim, M., Lee, K. G., Inam, M. A., Khan, I. A., Khan, R., et al. (2022). Use of ballasted flocculation (BF) sludge for the manufacturing of lightweight aggregates. *J. Environ. Manag.* 305, 114379. doi:10.1016/j.jenvman.2021.114379

Levins, D. M., and Smart, R. S. C. (1984). Effects of acidification and complexation from radiolytic reactions on leach rates of SYNROC C and nuclear waste glass. *Nature* 309, 776–778. doi:10.1038/309776a0

Li, J. Y., Li, J. X., Liu, X. L., Chen, J. C., Tian, P. F., Dai, S., et al. (2021). *Probing the role of surface hydroxyls for Bi, Sn and in catalysts during CO2 Reduction*, 298. Netherlands: Applied Catalysis B-Environmental.

Li, W. Z., Lutz, D. M., Wang, L., Takeuchi, K. J., Marschilok, A. C., Takeuchi, E. S., et al. (2021). Peering into batteries: Electrochemical insight through *in situ* and

operando methods over multiple length scales. *Joule* 5, 77–88. doi:10.1016/j.joule.2020.11.003

Li, Y. H., Wang, S. G., Cao, A. Y., Zhao, D., Zhang, X. F., Xu, C. L., et al. (2001). Adsorption of fluoride from water by amorphous alumina supported on carbon nanotubes. *Chem. Phys. Lett.* 350, 412–416. doi:10.1016/s0009-2614(01)01351-3

Li, Y., Yu, J. L., Liu, Y. X., Huang, R. K., Wang, Z. H., Zhao, Y. C., et al. (2022). A review on removal of mercury from flue gas utilizing existing air pollutant control devices (APCDs). *J. Hazard. Mater.* 427, 128132. doi:10.1016/j.jhazmat.2021.128132

Li, Z. H., Hu, K. M., Zhang, X. Q., Gong, L. X., Jiang, Z., Xing, Y. A., et al. (2022). Distributed treatment of rural environmental wastewater by artificial ecological geographic information system. *J. King Saud Univ. - Sci.* 34, 101806. doi:10.1016/j.jksus.2021.101806

Liao, X.-F., Zhong, J.-P., Chen, Y.-N., Qiu, T.-S., and Ren, S.-L. (2022). Preparation of functional attapulgite composite and its adsorption behaviors for Congo red. *Huan jing ke xue= Huanjing kexue* 43, 387–397. doi:10.13227/j.hjkx.202104304

Long, Z., Tong, X., Wang, R., Channa, A. I., Li, X., You, Y., et al. (2022). *Engineered environment-friendly colloidal core/shell quantum dots for high-efficiency solar-driven photoelectrochemical hydrogen evolution*. Weinheim: ChemSusChem.

Lopez, G., Santamaria, L., Lemonidou, A., Zhang, S., Wu, C., Sipra, A. T., et al. (2022). Hydrogen generation from biomass by pyrolysis. *Nat. Rev. Methods Prim.* 2, 20. doi:10.1038/s43586-022-00097-8

Lubkowicz, D., Horvath, N. G., James, M. J., Cantarella, P., Renaud, L., Bergeron, C. G., et al. (2022). An engineered bacterial therapeutic lowers urinary oxalate in preclinical models and *in silico* simulations of enteric hyperoxaluria. *Mol. Syst. Biol.* 18, e10539. doi:10.15252/msb.202110539

Lv, H., Qin, H., Ariga, K., Yamauchi, Y., and Liu, B. (2022). A general concurrent template strategy for ordered mesoporous intermetallic nanoparticles with controllable catalytic performance. *Angew. Chem. Int. Ed. Engl.* 134, e202116179. in English). doi:10.1002/ange.202116179

Mahfoudhi, N., and Boufi, S. (2020). Porous material from cellulose nanofibrils coated with aluminum hydroxyde as an effective adsorbent for fluoride. *J. Environ. Chem. Eng.* 8, 103779. doi:10.1016/j.jece.2020.103779

Morris, A. J., Oconnor, R., Holmes, R., Landes, D., Shah, K., Tanday, A., et al. (2022). Dental fluorosis. *Br. Dent. J.* 232, 492. doi:10.1038/s41415-022-4210-1

Mu, X., Yu, J., Leng, X., and Li, Y. (2022). Syndioselective coordination (Co) polymerization of triphenylamine-substituted styrenes via a scandium catalyst system. *Polym. J.* 54, 775–782. doi:10.1038/s41428-022-00628-w

Ni, H. J., Wu, W. Y., Lv, S. S., Wang, X. X., and Tang, W. J. (2022). Formulation of non-fired bricks made from secondary aluminum ash. *Coatings* 12, 2. doi:10.3390/coatings12010002

Ortiz-Gomez, I., Gonzalez-Alfaro, S., Sanchez-Ruiz, A., De Orbe-Paya, I., Capitan-Vallvey, L. F., and Navarro, A. Reversal of a fluorescent fluoride chemosensor from turn-off to turn-on based on aggregation induced emission properties. *Acs Sensors* 7, 37. doi:10.1021/acssensors.1c02196

Peters, K., Malfa, E., and Colla, V. (2019). *The european steel technology platform's strategic research agenda: A further step for the steel as backbone of EU resource and energy intense industry sustainability*. Italiana: Metallurgia Italiana, 5–17.

Qu, C. C., Yang, S. S., Mortimer, M., Zhang, M., Chen, J. Z., Wu, Y. C., et al. (2022). Functional group diversity for the adsorption of lead(Pb) to bacterial cells and extracellular polymeric substances. *Environ. Pollut.* 295, 118651. doi:10.1016/j.envpol.2021.118651

Qu, Z. B., Sun, F., Gao, J. H., and Zhao, G. B. (2022). Activity origin of boron doped carbon cluster for thermal catalytic oxidation: Coupling effects of dopants and edges. *J. Colloid Interface Sci.* 613, 47–56. doi:10.1016/j.jcis.2022.01.017

Querejeta, N., Rubiera, F., and Pevida, C. (2022). Experimental study on the kinetics of CO2 and H2O adsorption on honeycomb carbon monoliths under cement flue gas conditions. *ACS Sustain. Chem. Eng.* 10, 2107–2124. doi:10.1021/acssuschemeng.1c07213

Raghav, S., Jain, P., and Kumar, D. (2021). Assembly of cerium impregnated pectin/silica-gel biopolymeric material for effective utilization for fluoride adsorption studies. *Electr. Netw.* 50, 273–281. doi:10.1016/j.matpr.2021.06.327

Ren, Z. M., Shao, L. N., and Zhang, G. S. (2012). Adsorption of phosphate from aqueous solution using an iron-zirconium binary oxide sorbent. *Water Air Soil Pollut.* 223, 4221–4231. doi:10.1007/s11270-012-1186-5

Riddell, J. K., Malin, A. J., Flora, D., McCague, H., and Till, C. (2022). *Association of water fluoride and urinary fluoride concentrations with attention deficit hyperactivity disorder in Canadian youth*. Kidlington: Environment International, Vol. 161, 105190.

Silva, A. C., and Mello-Castanho, S. R. H. (2007). Vitrified galvanic waste chemical stability. *J. Eur. Ceram. Soc.* 27, 565–570. doi:10.1016/j.jeurceramsoc.2006.04.110

Song, W. X., Beigneux, A. P., Winther, A. M. L., Kristensen, K. K., Gronnemose, A. L., Yang, Y., et al. (2022). Electrostatic sheathing of lipoprotein lipase is essential for its movement across capillary endothelial cells. *J. Clin. Invest.* 132, e157500. doi:10.1172/jci157500

Su, Y., Cui, H., Li, Q., Gao, S. A., and Shang, J. K. (2013). Strong adsorption of phosphate by amorphous zirconium oxide nanoparticles. *Water Res.* 47, 5018–5026. doi:10.1016/j.watres.2013.05.044

Subbotina, E., Rukkijakan, T., Marquez-Medina, M. D., Yu, X., Johnsson, M., Samec, J. S. M., et al. (2021). Oxidative cleavage of C–C bonds in lignin. *Nat. Chem.* 13, 1118–1125. doi:10.1038/s41557-021-00783-2

Tripathy, S. S., Bersillon, J.-L., and Gopal, K. (2006). Removal of fluoride from drinking water by adsorption onto alum-impregnated activated alumina. *Sep. Purif. Technol.* 50, 310–317. doi:10.1016/j.seppur.2005.11.036

Ullah, Z., and Arslan, A. (2022), *R&D contribution to sustainable product attributes development: The complementarity of human capital*. Brazil: Sustainable Development.

Wagstaff, A., and Petrie, B. (2022). Enhanced desorption of fluoxetine from polyethylene terephthalate microplastics in gastric fluid and sea water. *Environ. Chem. Lett.* 20, 975–982. doi:10.1007/s10311-022-01405-0

Wang, G., Wang, A. C., Wang, E. H., Song, Y. D., Zou, Y. T., Duan, A. J., et al. (2022). DFT insights into competitive adsorption and reaction mechanism of benzothiophene and naphthalene on Fe-doped Ni2P catalyst. *Fuel* 314, 123114. doi:10.1016/j.fuel.2021.123114

Wang, W. D., and Cann, K. (2002). Carbon black used as a fluidization aid in gas phase elastomer polymerization: I. Carbon black-monomer interactions. *Carbon* 40, 221–224. doi:10.1016/s0008-6223(01)00178-6

Wang, X. Y., Shi, B. B., Yang, H., Guan, J. Y., Liang, X., Fan, C. Y., et al. (2022). Assembling covalent organic framework membranes with superior ion exchange capacity. *Nat. Commun.* 13, 1020. doi:10.1038/s41467-022-28643-8

Wang, Z., Lin, X., Huang, Y., and Ma, L. (2022). The role of hydroxylation on·OH generation for enhanced ozonation of benzoic acids: Reactivity, ozonation efficiency and radical formation mechanism. *J. Hazard. Mater.* 431, 128620. doi:10.1016/j.jhazmat.2022.128620

Wood, D., and Wilcox, D. (2022). Hypospadias: Lessons learned. An overview of incidence, epidemiology, surgery, research, complications, and outcomes. *Int. J. Impot. Res.* doi:10.1038/s41443-022-00563-7

Wu, F., Tian, H., Shen, Y., Hou, Z., Ren, J., Gou, G., et al. (2022). Vertical MoS2 transistors with sub-1-nm gate lengths. *Nature* 603, 259–264. doi:10.1038/s41586-021-04323-3

Xiao, Y., Liu, K., Hao, Q. C., Li, Y. S., Xiao, D., and Zhang, Y. J. (2022), *Occurrence, controlling factors and health hazards of fluoride-enriched groundwater in the lower flood plain of yellow river*. Northern China: Exposure and Health.

Xie, H., Xie, X., Hu, G., Prabhakaran, V., Saha, S., Gonzalez-Lopez, L., et al. (2022). Ta–TiOx nanoparticles as radical scavengers to improve the durability of Fe–N–C oxygen reduction catalysts. *Nat. Energy* 7, 281–289. doi:10.1038/s41560-022-00988-w

Xie, Z., Wang, P., Wang, X., Castro-Jiménez, J., Kallenborn, R., Liao, C., et al. (2022). *Organophosphate ester pollution in the oceans*. London: Nature Reviews Earth & Environment.

Xu, X. H., Li, Y. X., Zhou, L., Liu, N., and Wu, Z. Q. (2022). Precise fabrication of porous polymer frameworks using rigid polyisocyanides as building blocks: From structural regulation to efficient iodine capture. *Chem. Sci.* 13, 1111–1118. doi:10.1039/d1sc05361b

Yang, D. H., Tao, Y., Ding, X. S., and Han, B. H. (2022). Porous organic polymers for electrocatalysis. *Chem. Soc. Rev.* 51, 761–791. doi:10.1039/d1cs00887k

Yang, M. Y., Chen, L., Msigwa, G., Tang, K. H. D., and Yap, P. S. (2022). *Implications of COVID-19 on global environmental pollution and carbon emissions with strategies for sustainability in the COVID-19 era*. Amsterdam: Science of the Total Environment, 809.

Yang, S., Geng, Q., Yang, C., Fan, H. L., Liang, M. S., Lei, J. X., et al. (2022). Insight into the influence of Ni2+ doping on the room temperature desulfurization/

regeneration performance of ZnO supported MCM-41 adsorbents. *Fuel* 313, 122694. doi:10.1016/j.fuel.2021.122694

Yang, T., Han, C. Y., Liu, H., Yang, L., Liu, D. K., Tang, J., et al. (2019). Synthesis of Na-X zeolite from low aluminum coal fly ash: Characterization and high efficient As(V) removal. *Adv. Powder Technol.* 30, 199–206. doi:10.1016/j.apt.2018.10.023

Yu, S. H., Dong, X. L., Gong, H., Jiang, H., and Liu, Z. G. (2012). Adsorption kinetic and thermodynamic studies of phosphate onto tantalum hydroxide. *Water Environ. Res.* 84, 2115–2122. doi:10.2175/106143012x13415215906933

Yuan, Y., Li, Y. J., Duan, L. B., Liu, H. T., Zhao, J. L., Wang, Z. Y., et al. (2018). CaO/Ca(OH)(2) thermochemical heat storage of carbide slag from calcium looping cycles for CO2 capture. *Energy Convers. Manag.* 174, 8–19. doi:10.1016/j.enconman.2018.08.021

Zeng, C., Liu, P., Xiao, Z. L., Li, Y., Song, L. B., Cao, Z., et al. (2022a). Highly selective adsorption and recovery of palladium from spent catalyst wastewater by 1, 4, 7, 10-tetraazacyclododecane-modified mesoporous silica. *ACS Sustain. Chem. Eng.* 10, 1103–1114. doi:10.1021/acssuschemeng.1c05915

Zeng, C., Liu, P., Xiao, Z. L., Li, Y., Song, L. B., Cao, Z., et al. (2022b), *Highly selective adsorption and recovery of palladium from spent catalyst wastewater by 1,4,7,10-tetraazacyclododecane-modified mesoporous silica*. America: Acs Sustainable Chemistry & Engineering.

Zhang, G. H., Xue, P., Wei, J., Zhang, Y. H., Zhao, L., Gao, J. S., et al. (2022). Competitive adsorption mechanism of thiophene with diethyl sulfide in Y zeolite: Displacement and migration. *Chem. Eng. J.* 435, 135141. doi:10.1016/j.cej.2022.135141

Zhang, H. L., Zhang, K., Wang, G. W., Tang, N., Zhu, X. L., Li, C. Y., et al. (2022). Propane dehydrogenation over core-shell structured Al2O3@Al via hydrothermal oxidation synthesis, *Fuel*, 312. 122756, doi:10.1016/j.fuel.2021.122756

Zhang, H. S., Hu, X., Li, T. X., Zhang, Y. X., Xu, H. X., Sun, Y. Y., et al. (2022). MIL series of metal organic frameworks (MOFs) as novel adsorbents for heavy metals in water: A review. *J. Hazard. Mater.* 429, 128271. doi:10.1016/j.jhazmat.2022.128271

Zhang, X. R., Guo, J. G., and Zhou, L. J. (2022). Experimental and theoretical investigation on the adsorption properties of benzene on graphene surface: Influence of pH and edge effects. *Chem. Eng. J.* 440, 135794. doi:10.1016/j.cej.2022.135794

Zhang, Z. B., Xia, Y., Wan, S. Y., Yang, D., and Dong, A. G. (2022). Confinement assembly in polymeric micelles enables nanoparticle superstructures with tunable molecular-like geometries. *Small Methods* 6, 2200014. doi:10.1002/smtd.202200014

Zhao, S. L., Luo, H., Ma, A. J., Xie, W., Sun, K., Sun, Z. Q., et al. (2022). Mercury removal by the S2Cl2 modified biomass coke with mechanochemical versus impregnation method. *Chem. Eng. J.* 435, 135073. doi:10.1016/j.cej.2022.135073

Zhou, S. L., Zhang, L. L., Mi, W. M., and Long, H. D. (2011). "Research on the recovery of mineral resource and the utilization of solid waste," in 3rd International Symposium on Environmental Science and Technology (2011 ISEST), Singapore, 28th February 2011 (Beijing: Dongguan PEOPLES R CHINA), 922–927.

Zhou, W. G., Zhang, Y. P., and Salanne, M. (2022). Effects of fluoride salt addition to the physico-chemical properties of the MgCl2-NaCl-KCl heat transfer fluid: A molecular dynamics study. *Sol. Energy Mater. Sol. Cells* 239, 111649. doi:10.1016/j.solmat.2022.111649

Zhu, T., Tian, M. L., and Row, K. H. (2010). Comparison of adsorption equilibrium of glycyrrhizic acid and liquiritin on C-18 column. *J. Industrial Eng. Chem.* 16, 929–934. doi:10.1016/j.jiec.2010.09.005

Zhu, X. L., Guo, Z. H., Yang, W., and Song, W. J. (2022). Durability of concrete with coal gasification slag and coal gangue powder. *Front. Mat.* 8. doi:10.3389/fmats.2021.791178

Conflict of Interest: The authors declare that the research was conducted in the absence of any commercial or financial relationships that could be construed as a potential conflict of interest.

Publisher's Note: All claims expressed in this article are solely those of the authors and do not necessarily represent those of their affiliated organizations, or those of the publisher, the editors and the reviewers. Any product that may be evaluated in this article, or claim that may be made by its manufacturer, is not guaranteed or endorsed by the publisher.